"Creative" Agentic AI solving open problems in Mathematics?

– The Direct Pathway to Advanced Artificial Super Intelligence (AASI) –*

Prof. Dr. V. David Sánchez A., Ph.D.
Brilliant Brains, Arlington, VA, Washington DC Metro
October 2026

Abstract

David Hilbert presented 10 of a list of 23 unsolved problems [4] at that time in his talk "Mathematische Probleme ("The Problems of Mathematics") at the 2nd International Congress of Mathematicians in Paris on August 8, 1900. The 23 problems belong to different categories in mathematics including foundations of mathematics and mathematical logic (Table 1), number theory (Table 2), algebra and geometry (Table 3), and mathematical analysis and mathematical physics (Table 4). In his working notes, he had written down 24 problems. The 24th problem is about a theory of the simplest proof. W.r.t. the primary branches of mathematics, the International Mathematical Union (IMU), the world's umbrella organization of the national mathematics organizations, its members, hosts every 4 years the International Congress of Mathematicians (ICM) and its scientific program is subdivided in sections. The last one took place in 2026 and its 20 sections are listed in Table 5. A granular Mathematics Subject Classification (MSC) System in its most recent version can be consulted in [5]. The world's most prestigious awards also provide hints about the most complex challenges in mathematics and the recognition for specific contributions. For example, one of the world's most prestigious age-independent mathematics awards is the Abel Prize [6], awarded yearly. The Fields Medal [7], awarded every four years, is considered the most prestigious distinction for mathematicians under the age of 40 for major discoveries. The Millennium Prize is tied to a specific mathematics problem and awarded by the Clay Mathematics Institute (CMI) for the solution of a given problem, 7 in total, only 1 so far solved. The Breakthrough Prize [8] is awarded yearly recognizing top scientists across three primary fields: life sciences, fundamental physics, and mathematics.

The Norwegian Academy of Science and Letters awarded Gerd Faltings the 2026 Abel Prize for introducing powerful tools in arithmetic geometry and resolving long-standing diophantine conjectures of Mordell and Lang. In 2026, IMU awarded 4 Field Medals, to (1) Y. Den for his work in partial differential equations, including the rigorous derivation of the Boltzmann equation from hard-sphere dynamics for rarefied gases, the derivation of wave kinetic equations from nonlinear dispersive systems, and probabilistic approaches to nonlinear Schrödinger dynamics; (2) J. Pardon for his achievements in symplectic geometry including new approaches to virtual fundamental cycles,

*This abstract has been granted permission for public release. The author has among many others a 15-year tenure as founding Chief Scientist/EiC of an Elsevier Science's AI/ML journal [1] and is the youngest "Nobel"-Prize in Engineering (IEEE Fellow) in history worldwide with the following mention "for leadership in neural and parallel computation, and pioneering contributions to autonomous space robots" [2]. As a decade civil servant at the German Aerospace Center DLR, he launched with the Office of the German Federal Minister of Research and Technology the First Federal Program for AI/ML Research and Technology Development in Germany [3], which funded multiple consortia all over the country, one of them being his consortium including DLR and Siemens Corporate R&D in Munich, Germany. He has been conceiving, designing, building, and operating advanced scalable mission-critical parallel and distributed as well as secure (NSA, commercial) computer systems for federal and state governments and the commercial industry, e.g., AI pipelines deployed to and executing during NASA-ESA-DLR spaceflight missions, ML pipelines for DoD classified programs, advanced AI/ML pipelines for advanced data centers and vertical on-prem, hybrid, and in the cloud applications including GenAI and agentic AI solutions.

Table 1: Hilbert's Problems – Foundations of Mathematics and Mathematical Logic, I of IV Categories

#	Name	Subdiscipline
1	Continuum Hypothesis	Set Theory and Mathematical Logic
2	Consistency of Arithmetic	Proof Theory and Mathematical Logic
24	Simplicity of Proofs - Omitted	Proof Theory, Automated Reasoning, and Mathematical Logic

Table 2: Hilbert's Problems – Number Theory, II of IV Categories

#	Name	Subdiscipline
7	Irrationality and Transcendence	Algebraic Number Theory and Transcendental Number Theory
8	Riemann Hypothesis & Prime Numbers	Analytic Number Theory
9	General Reciprocity Laws	Algebraic Number Theory
10	Solvability of Diophantine Equations	Computability Theory and Number Theory
11	Quadratic Forms with Algebraic Coefficients	Arithmetic Geometry and Number Theory
12	Kronecker's Theorem Extension	Algebraic Number Theory and Arithmetic Geometry

Table 3: Hilbert's Problems – Algebra and Geometry, III of IV Categories

#	Name	Subdiscipline
3	Volumes of Tetrahedra	Discrete Geometry and Topology
4	Straight Line as Shortest Distance	Differential Geometry and Foundations of Geometry
5	Lie Groups without Differentiability Assumptions	Continuous Transformation Groups and Topological Groups
13	Impossibility of Solving 7th Degree Equations with 2-Variable Functions	Algebraic Geometry and Approximation Theory
14	Finiteness of Linear Invariant Systems	Commutative Algebra and Invariant Theory
15	Rigorous Foundation of Schubert's Enumerative Calculus	Algebraic Geometry
16	Topology of Algebraic Curves and Surfaces	Real Algebraic Geometry and Topology
17	Expression of Definite Forms by Squares	Real Algebra and Field Theory
18	Building Space from Polyhedra / Kepler Conjecture	Discrete Geometry and Tesselation

Table 4: Hilbert's Problems – Mathematical Analysis and Mathematical Physics, IV of IV Categories

#	**Name**	**Subdiscipline**
6	Axiomatization of Physics	Mathematical Physics and Probability Theory
19	Analyticity of Extremal Solutions	Calculus of Variations and Partial Differential Equations (PDEs)
20	General Boundary Value Problems	Partial Differential Equations (PDEs)
21	Linear Differential Equations with a Monodromy Group	Complex Analysis and Ordinary Differential Equations (ODEs)
22	Uniformization of Analytic Relations	Complex Analysis and Riemann Surface Theory
23	Further Development of the Calculus of Variations	Further Development of the Calculus of Variations

Fukaya categories of certain manifolds and counting holomorphic curves, and for his contributions to other areas of geometry and topology, including group actions on 3-manifolds and knot theory; (3) J. Tsimerman for his contribution in the recasting of o-minimality as a fundamental method of arithmetic and complex algebraic geometry, and his role in the proof of many central conjectures including Griffiths' conjecture on the algebraicity of images of the period maps, and the André-Oort conjecture for Siegel modular varieties; and (4) H. Wang for her work in harmonic analysis and geometric measure theory, including applications of multiscale and decoupling techniques to the local smoothing conjecture for the planar wave equation, and major advances in Fourier restriction, Falconer distance sets, Furstenberg sets in the plane, and the Kakeya problem in three dimensions. On March 18, 2010, CIM awarded Grigoriy Perelman the Millennium Prize for the resolution of the Poincaré Conjecture, which he declined. The 2026 Breakthrough Prize in Mathematics was awarded to Frank Merle for breakthroughs in nonlinear evolution equations, with regards to their stability, singularity formation, or resolution into solitons. Apart from awards and public recognition that have proliferated in recent times, the work of history's preeminent mathematicians including Euclid, Archimedes, Descartes, Pascal, Leibniz, Newton, Euler, Laplace, Fourier, Galois, Gauss, Lobachevsky, Cauchy, Chebyshev, Hilbert, Kolmogorov has predominantly eclipsed the work of peers by its paradigm-shifting scope, raw structural intuition, and foundational creation.

Creativity means, quite simply, the ability to create or the quality of being creative. And by create, we specifically mean to make, form, build or bring something new into existence through imaginative skill. That means something unique using imagination rather than just copying an existing process. Some of the most well-accepted areas of human activity that require creativity are the sciences and the arts, i.e., the work performed by professional scientists and artists. In particular by abstract mathematicians, specifically for instance to perform formal proving of novel theorems, considered open problems in mathematics. For comprehensive details regarding my work in multiple areas of advanced mathematics developing sophisticated mathematical frameworks—including formal proofs and the efficient management of NP-hard problems—please refer to [9]. This pioneering AI research and technology development work, initiated way ahead of its time, has successfully continued since the 1980s, and has transitioned fluently in every case from its advanced mathematics and computer science to mature, production-grade AI engineering systems. These systems have been robustly deployed across mission-critical sectors within both private industry and government agencies. To start motivating the presentation of ideas including the use of the state-of-the-art tools, let us take one of the most famous results in mathematics, The Pythagorean theorem [10] is a fundamental relation in Euclidean geometry between the three sides a, b, c of a right triangle. It states that the area of the square whose side is the hypotenuse c, the side opposite the right angle, is equal to

Table 5: International Mathematical Union (IMU) – International Congress of Mathematicians (ICM) 2026 – Scientific Program sections

#	**ICM 2026 Sections**
1	Logic
2	Algebra
3	Number Theory
4	Algebraic and Complex Geometry
5	Lie Theory and Generalizations
6	Topology
7	Differential Geometry and Its Applications
8	Analysis and Operator Algebra
9	Ordinary Differential Equations and Dynamical Systems
10	Partial Differential Equations
11	Mathematical Physics
12	Probability and Statistics
13	Combinatorics
14	Numerical Analysis and Scientific Computing
15	Computer Science in Mathematics
16	Control Theory and Optimization
17	Applications of Mathematics in the Sciences
18	History of Mathematics
19	Mathematics Education
20	General and Miscellaneous / Popularization of Mathematics

Table 6: Millennium Prize Problems

#	**Name**	**Primary Category**
1	P versus NP Problem	Computer Science / Discrete Mathematics
2	Riemann Hypothesis	Pure Mathematics / Number Theory
3	Poincaré Conjecture	Pure Mathematics / Geometry & Topology
4	Birch and Swinnerton-Dyer Conjecture	Pure Mathematics / Number Theory & Arithmetic Geometry
5	Hodge Conjecture	Pure Mathematics / Geometry
6	Navier–Stokes Existence and Smoothness	Applied Mathematics / Mathematical Physics
7	Yang–Mills Existence and Mass Gap	Mathematical Physics / Pure Mathematics

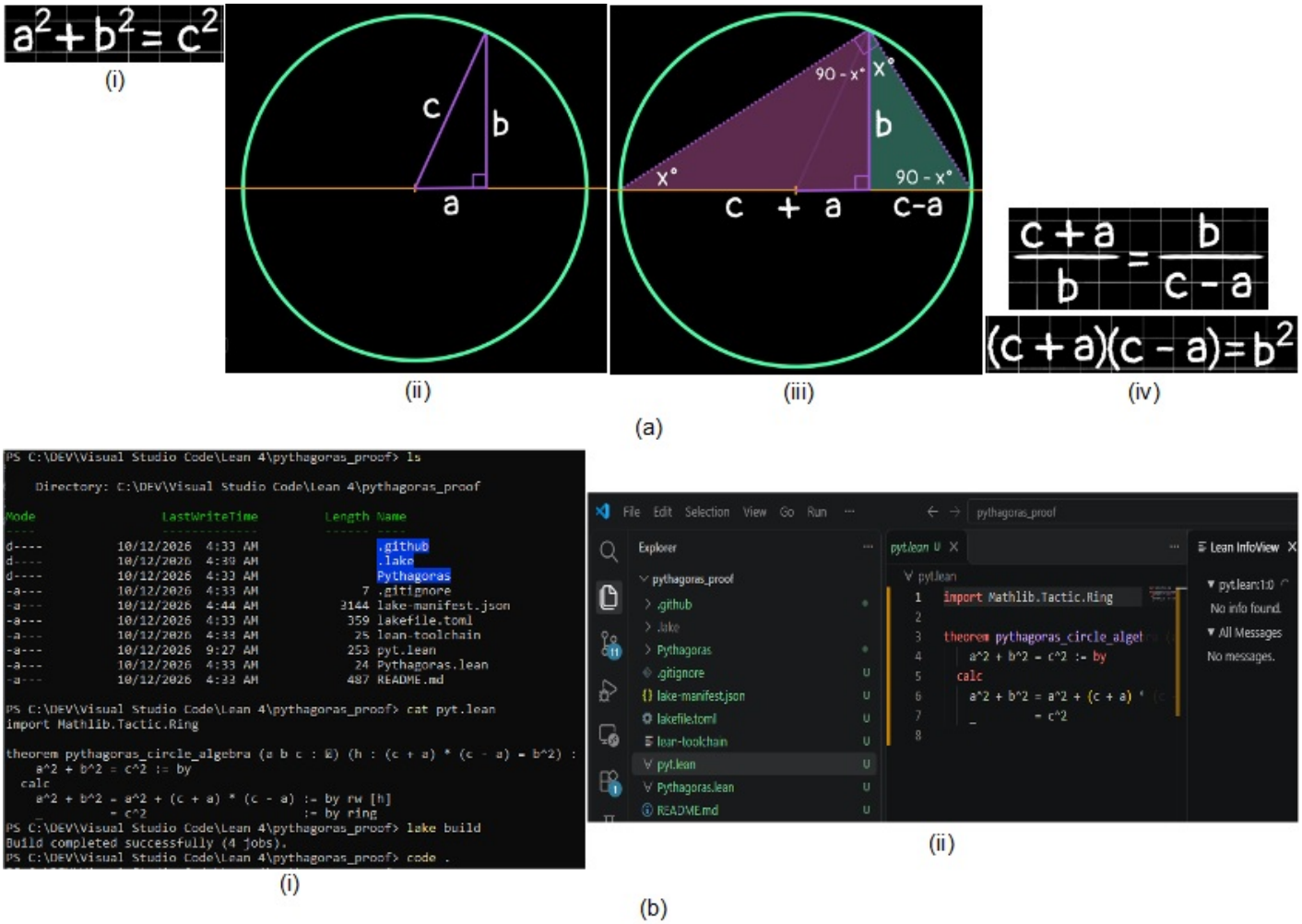

Figure 1: The Pythagorean Theorem and Its Proof (one of many) (a) the equation to be proved and transformations of this initially circular geometric proof (b) Formal verification of the algebraic finalization steps using Lean 4

the sum of the areas of the squares on the other two sides a, b which are called legs of the triangle, i.e., in algebraic terms: $c^2 = a^2 + b^2$ which is the Pythagorean equation. Triples (a, b, c) that satisfy the Pythagorean theorem are called Pythagorean triples, see Figure 1(a) for the equation (i) that needs to be proved and some geometric constructions (ii–iv) that conceptually lead to a solution, i.e., to a circular geometric proof of the theorem. There are hundreds of proofs of the Pythagorean theorem. Figure 1(b) shows the formal verification of the algebraic finalization steps of that proof of the Pythagorean theorem using the difference of squares and using the tool called Lean [11] (latest stable version 4.34.1), which is an open-source programming language and proof assistant, in the Power Shell (i) and the Visual Studio Code (ii) environments. We now briefly define the logic for a proof by counterexample which uses a single specific instance to show that a universal statement is false. Let us assume that the target statement is a universal claim asserting that a condition holds true for every element of a domain: $\forall x P(x)$ or $\forall x(P(x) \rightarrow Q(x))$. The logical negation of that target statement is the existential statement: $\exists x \neg P(x)$ or $\exists x(P(x) \wedge \neg Q(x))$. During the proof step, to prove the negation is true, breaking the universal claim, only one element (x) is needed, needs to be generated/shown, where the hypothesis (P(x)) is true and the conclusion (Q(x)) is false. Figure 2(a) shows an introductory instance of a proof by counterexample: how to prove that the claim P(n) = "For every integer $n, n^2 = n$" is false, or equivalently, disprove that claim. We use Lean 4 for that purpose, the counterexample used is $n = 2$.

The recent solution to open problems in advanced mathematics accomplished by human math-

ematicians with and without AI support are discussed next including the unit distance conjecture, the Poincaré conjecture, and the existence of smooth solutions to the Navier–Stokes equation. The indispensable use of creativity to bring new frameworks (tools) into existence in order to solve some open problems is highlighted discussing the Ricci's calculus, needed for the theory of general relativity to solve Einstein's field equations, and the Ricci flow to resolve the Poincaré conjecture. Because topological behavior varies drastically with a space's dimension, the generalized Poincaré conjecture was not solved sequentially with increasingly higher dimensions. While the lower dimensions ($n = 1, 2$) fell first, the high-dimensional versions ($n \geq 5$, followed by $n = 4$) were actually proven before the notoriously difficult $n = 3$ case originally posed by Poincaré in 1904. And more importantly, that is the reason why entirely new mathematical tools needed to be invented, for which purpose lots of creativity is indispensable. One event that is being considered as the first time AI can perform or potentially even outperform human performance in formal proving of open problems in abstract mathematics happened this year 2026. The unit distance conjecture [12], the best-known open problem in discrete combinatorial geometry, states: Given a finite set of n points $P \subset \mathbb{R}^2$, let the number of unordered unit-distance pairs in P be: $\nu(P) = \#\{\{x, y\} \subset P : |x - y| = 1\}$, and let the maximum of $\nu(P)$ over all n-point planar sets be: $\nu(n)$. There should be an absolute constant C such that, for all sufficiently large $n : \nu(n) \leq n^{1+\frac{C}{\log\log n}}$. This conjecture has recently, in May 2026, been disproved using AI operating autonomously according to [13], by proving that there exists an absolute constant $\delta > 0$ and infinitely many positive integers n for which $\nu(n) \geq n^{1+\delta}$, that is, using a proof by counterexample. The solution was delivered by a new general-purpose reasoning AI model, rather than from a system trained specifically for mathematics, by a so called internal AI model, unavailable to the public. Given to this model was a prompt, cf. Figure 2(b), containing an AI-written statement of the problem. Its output was sent to an AI grading pipeline, which indicated high confidence that the solution was correct. At this point, human mathematicians examined the solution carefully and after a preliminary AI-assisted verification and rewriting, a draft was sent to external experts including number theorists who confirmed the correctness of the proof created by the autonomous AI model. One basic key idea of the solution is to construct counterexamples using algebraic number fields. The proof falls into two parts: (1) an arithmetic part to construct the required fields using an infinite unramified pro-3 quotient tower following class-field-theoretic methods [15, 16] and (2) proving a geometric criterion: given suitable number fields F_j and split rational primes q_b, fixed independently of j, it constructs the planar point sets by embedding norm-one elements into a high-dimensional Minkowski lattice, cutting by a product of discs, and projecting to the first complex coordinate. K being a number field, the class-number $h(K)$ [17][section I.6] estimate in part (1) gives the uniform exponential bound needed in the geometric criterion, part (2).

Figure 3 helps visualize, explain the unit distance conjecture. To calculate the lower bound on the number of unit-distance lines for n points, the points are laid out in a grid as shown in Figure 3(a). The black circle shows a set of 12 neighbor points, from which the unit distances are built. It is not an optimal layout, but if points in a grid have a certain number of pairs with unit distance, then an optimal layout must have at least that number. Pythagorean triangles are well-known geometric figures. For example, the one with legs of $a = 3$ and $b = 4$ and a hypotenuse of $c = 5$. According to the Pythagorean theorem: $a^2 + b^2 = c^2$ or in this case $3^2 + 4^2 (= 9 + 16) = 5^2 (= 25)$. That Pythagorean triangle can be embedded in a circle of radius 5. To make the explanation easier to follow, let us consider a circle with center at $(0, 0)$ of radius 5. The 12 neighbor points all belonging to the circle can be generated as follows: In the first quadrant: $(5, 0), (4, 3)$, and $(3, 4)$. In the second quadrant: $(0, 5), (-3, 4)$, and $(-4, 3)$. In the third quadrant: $(-5, 0), (-4, -3)$, and $(-3, -4)$. In the fourth quadrant: $(0, -5), (3, -4)$, and $(4, -3)$. To make the distance between neighbor points equal to the unity, we need to actually divide all coordinates of the so far generated points by 10 (twice the radius of 5). Hence, for example, the distance between neighbor point $(-3, 4)/10$ (2nd quadrant) and the neighbor point $(3, -4)/10$ (4th quadrant) becomes $(\sqrt{(-3-(3))^2 + (4-(-4))^2})/10 = (\sqrt{(-6)^2 + (8)^2})/10 = (\sqrt{36+64})/10 = (\sqrt{100})/10 = 10/10 = 1$. This is one of the 6 unit distances shown in red. Presented here is only one frame of an animation showing how the black circle with its 6 red unit distances wanders from one end to the other end of the grid. Figure 3(b) shows some of the

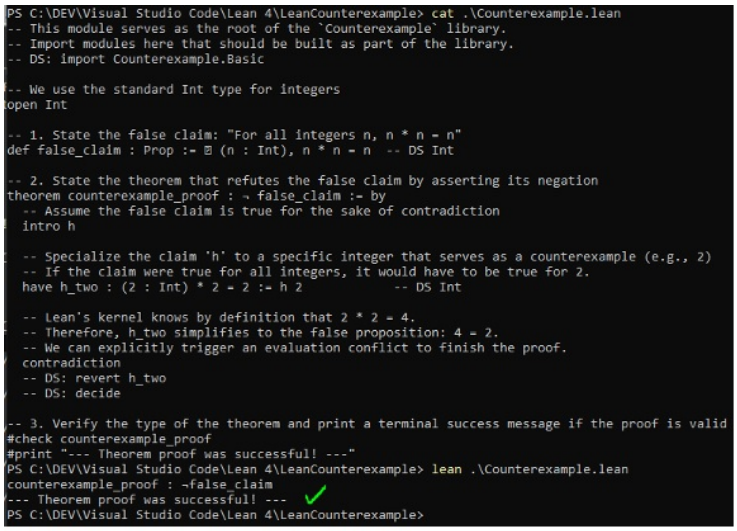

(a)

Prompt.

Let $P \subset \mathbb{R}^2$ be a finite set of distinct points. Define

$$\nu(P) = \left| \left\{ \{p, q\} \in \binom{P}{2} : \|p - q\|_2 = 1 \right\} \right|$$

and, for each integer $n \geq 1$, $\nu(n) = \max_{\substack{P \subset \mathbb{R}^2 \\ |P|=n}} \nu(P)$.

Resolve Erdős's planar unit-distance problem completely: $\nu(n) \leq n^{1+O(1/\log\log n)}$ as $n \to \infty$? Equivalently, determine whether there exist absolute constants $C > 0$ and $N \in \mathbb{N}$ such that $\nu(n) \leq n^{1+C/\log\log n}$ for every integer $n \geq N$. Here log denotes the natural logarithm, and N may be taken large enough that $\log\log n > 0$. The hidden constant in $O(1/\log\log n)$ is absolute and independent of P and n.

A complete solution must prove exactly one of the following.

Affirmative resolution. Prove that there exist absolute constants $C > 0$ and $N \in \mathbb{N}$ such that every set $P \subset \mathbb{R}^2$ of $n \geq N$ distinct points satisfies $\nu(P) \leq n^{1+C/\log\log n}$.

Negative resolution. Prove that no such constants exist. Equivalently, prove that for every $C > 0$ and every $N \in \mathbb{N}$, there are an integer $n \geq N$ and a set $P \subset \mathbb{R}^2$ of n distinct points such that $\nu(P) > n^{1+C/\log\log n}$.

Pairs are unordered, the distance is the usual Euclidean distance in $\mathbb{R}^2$, and the asymptotic assertion is for all sufficiently large integers n, not merely infinitely many n.

Partial progress does not count unless it implies one of the two resolutions above. In particular, improved bounds such as $O(n^{4/3-\varepsilon})$, better constants in the $n^{4/3}$ bound, finite verification, special cases, structural reductions, or heuristic evidence are insufficient unless they prove the full Erdős bound or disprove it.

(b)

Figure 2: Advanced AI tools (a) Proof by Counterexample, instance formalizing verification using the Lean 4 tool (b) Prompt given to OpenAI internal AI model that solved the unit distance conjecture [14]

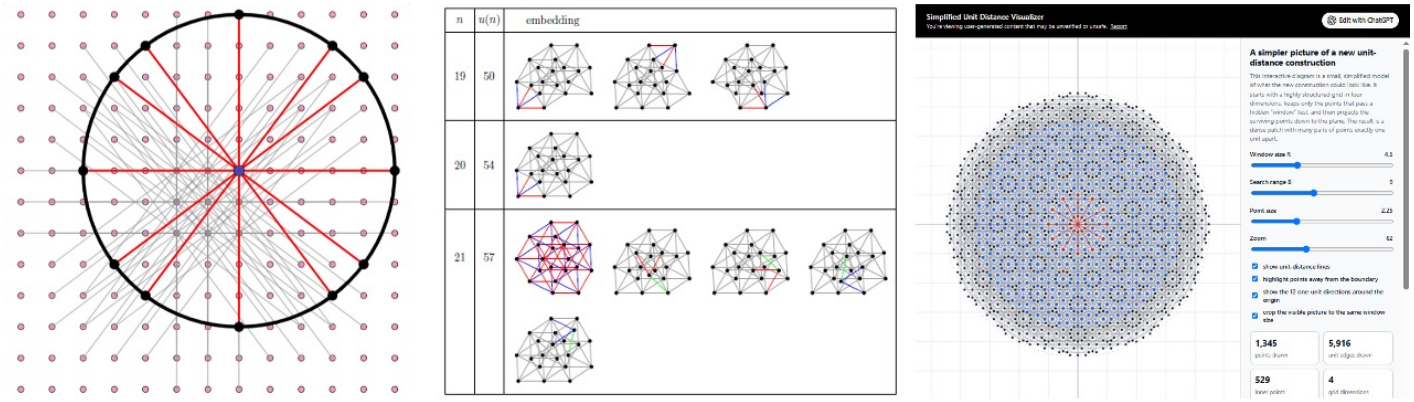

(a) (b) (c)

Figure 3: The unit distance conjecture (a) grid layout for lower bound calculation (b) some unit-distance graphs from [18] (c) simplified model to explain new unit-distance construction [19]

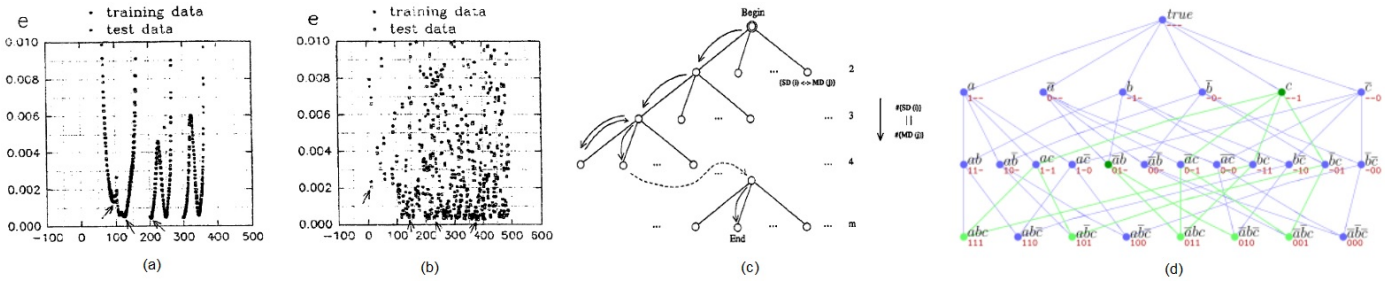

Figure 4: Searching for a problem solution, solutions found within and with AI (a) foundations from computational learning theory (CoLT) (solution without index ordering) [20] (b) i.e., discrete mathematics and combinatorics, probability and statistics, functional analysis and approximation theory. complexity theory (solution with index ordering) [21] (c) generic goal of reaching the final state from a begin state in some optimal fashion via advanced search including AI heuristics [22] (d) foundations from abstract order theory, lattice theory (in general NP-hard, NP-complete problem) [23]

densest unit-distance graphs (embeddings) with n vertices and $u(n)$ edges on at most 21 vertices [18]. When growing from smaller to larger embeddings, new edges are drawn in different color. Figure 3(c) shows an interactive diagram created by a small, simplified model [19] of what the new construction could look like. It starts with a highly structured grid, keeps only the points that pass a hidden window test, and then projects the surviving points down to the plane. The result is a dense patch with pairs of points exactly one unit apart from each other. This event accentuates the relevance and convenience of using AI as powerful "creative" assistant, in particular due to its brute force, i.e., computational power behind AI due to specialized hardware to search more options along the way to the final solution in less amount of time than human-counterparts can handle. Partly due to that lack of computational power and human resources, a "common" belief had been that this particular conjecture, i.e. the bound as originally stated $n^{1+o(1)}$, was "probably" true. In the particular case of the solution to the unit distance conjecture, humans typically do not explore massive solution spaces where there are too many decisions to make along the way to a proof. AI on the other hand was able to explore these possibilities much more comprehensibly and found a path to the solution. It is gratifying to observe that the global AI, mathematics, and computer science communities are now finally, increasingly arriving at these foundational insights that I have been intimately applying to my own AI work since the 1980s. Figure 4 shows two examples: (1) during the fully automatic design of artificial brains (a, b) [20], please relate it to "Training a 3-Node Neural Network is NP-Complete" in [24] or "The perceptron has shown itself worthy of study (and even because of!) its severe limitations. It has many features to attract attention: its linearity; its intriguing learning theorem; its clear paradigmatic simplicity as a kind of parallel computation. There is no reason to suppose that any of these virtues carry over to the many-layered version. Nevertheless, we consider it to be an important research problem to elucidate (or reject) our intuitive judgment that the extension is sterile" from [25][chapter 13.2], and (2) while solving NP-complete problems to a degree with AI (c, d) [23], for further details see [9], please relate it to the Quine–McCluskey (QMC) method of prime implicants [26, 27] with a time complexity bound of $O(\frac{3^n}{\sqrt{n}})$ for generating prime implicants for n variables [28] and the NP-completeness of the covering step in [29].

Let us now discuss Ricci's calculus. In the same or similar way in which ordinary calculus works well in the Euclidian (flat) space, a form of calculus was needed that works in curved spaces, handles transformations consistently and curvature naturally. Ricci's calculus, a tensor analysis, was introduced for that purpose in [30]. Figure 5 shows some of its basic features starting with the concept of tensor and its operations. It extended classical calculus to curved spaces and coordinate-independent geometric structures. The basic vectors of Riemannian manifolds (curved space) may vary from place to place. That space's geometry is described by a metric tensor. In particular, the Ricci tensor represents a specific contraction of the Riemann curvature tensor that measures how a geometric volume changes along geodesics compared to standard Euclidean space. To account for how coordinate axes twist and bend in curved space, a covariant differentiation is introduced

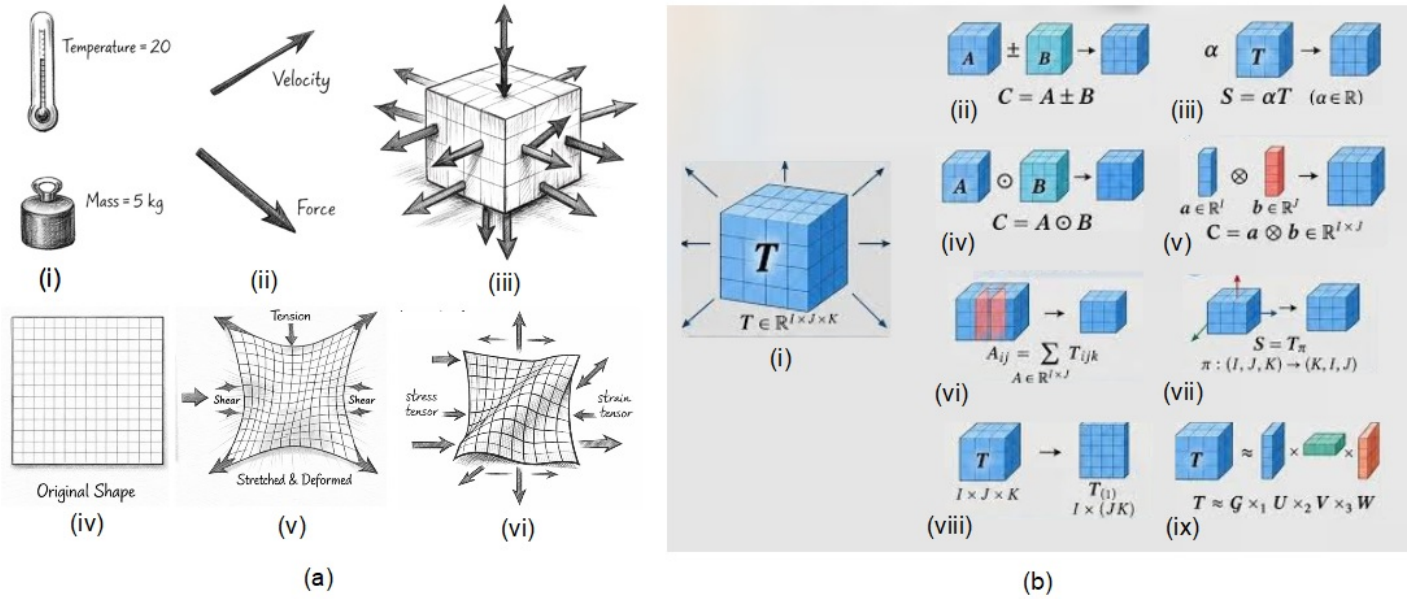

Figure 5: Ricci's calculus (a) Tensor concept: (i) scalar (ii) vector (iii) tensor (iv) original grid (v) stretched & deformed grid (vi) stress & strain tensors – (b) Tensor operations: (i) tensor (ii) add & subtract (iii) scalar multiply (iv) Hadamard product (v) outer product (vi) contraction (vii) index permutation (viii) reshape & unfold (ix) decomposition

instead of the standard derivative. Applications have included for example its use in the theory of general relativity where the universe is modeled as a 4-dimensional manifold (one time and three spatial dimensions). The Einstein field equations directly equate the Ricci curvature tensor to the distribution of matter and energy. The Ricci curvature tensor measures how the volume of a small region of curved spacetime changes relative to flat space as geodesics (paths of free fall) converge or diverge. In index-free notation: $\mathbf{G} = \mathbf{R} - \frac{1}{2}\mathbf{g}R$ with $\mathbf{R}, \mathbf{g}, \mathbf{G}$ being the Ricci, metric, and Einstein tensors, respectively, and R is the scalar curvature defined as the trace of the Ricci curvature tensor $\mathbf{R}$ w.r.t. $\mathbf{g}$ the metric tensor: $R = \mathrm{Tr}_{\mathbf{g}}(\mathbf{R})$. Or in component form: $G_{\mu\nu} = R_{\mu\nu} - \frac{1}{2}g_{\mu\nu}R$. In n dimensions, contracting the equation and simplifying yields: $G = \frac{2-n}{2}R$ for the traces. In particular, relevant for general relativity with $n = 4$ dimensions: $G = -R$, with G, R being the traces of the Einstein and Ricci tensors respectively, that is why the Einstein tensor is also called the trace-reverted Ricci tensor.

In general relativity, the field equations take the form: $\mathbf{G} + \Lambda\mathbf{g} = \kappa\mathbf{T}$ with Λ, κ being the cosmological constant and the Einstein gravitational constant (a coupling constant), respectively. Btw., $\kappa = \frac{8\pi G}{c^4}$ with G, c being the Newtonian gravitational constant and the speed of light in vacuum, respectively. The left side of the field equation is an expression of spacetime geometry including its curvature, i.e., how spacetime is bent. The right side is an expression of the stress, energy and momentum as source of the gravity, i.e., what causes the bending. Internal stresses include pressure and shear. Mass is a concentrated form of energy $E = mc^2$. Matter is described macroscopically by what kind of energy and momentum it carries through spacetime, that includes dust, fluids, gases, or electromagnetic radiation. $\mathbf{G}$ represents the overall curvature of spacetime, measures the actual geometric warping of spacetime, that is, the stretch, squeeze, and tidal distortions. $\Lambda\mathbf{g}$ is a cosmological constant term. $\mathbf{g} = (g_{\mu\nu})$ is a rank-2, covariant, symmetric tensor field defined over a 4-dimensional spacetime manifold, fundamental to measure distances, angles, and times in the curved spacetime. The metric tensor is typically written as a symmetric 4 matrix and has therefore $10 = 4 + \frac{16-4}{2}$ independent components. Λ represents the energy density of the empty spacetime, today used to describe dark energy, the force responsible for the universe's accelerating expansion. $\mathbf{T}$ is the stress-energy-momentum tensor, whose components below measure along each individual coordinate axis (x, y, z) are defined using:

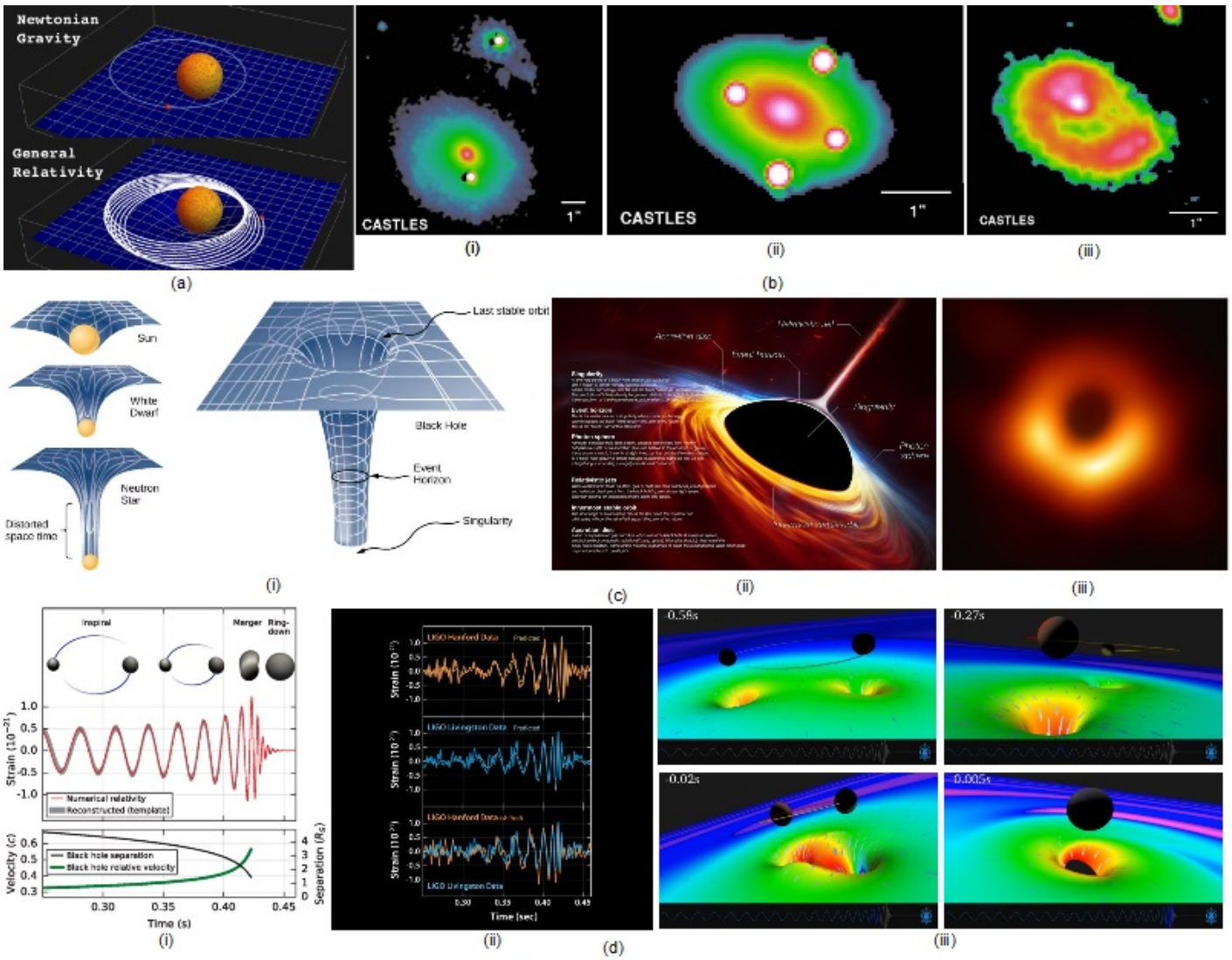

Figure 6: Empirical validation of general relativity (a) Mercury's orbital precession (b) Gravitational Lensing [CfA] (c) Black Holes [NASA] (d) Gravitational Waves [Caltech, MIT]

$$\mathbf{T} = (T_{\mu\nu}), \mu, \nu \in \{0, \cdots, 3\} = \begin{pmatrix} T_{00} & T_{01} & T_{02} & T_{03} \\ T_{10} & T_{11} & T_{12} & T_{13} \\ T_{20} & T_{21} & T_{22} & T_{23} \\ T_{30} & T_{31} & T_{32} & T_{33} \end{pmatrix}$$

$$= \begin{pmatrix} \text{Energy Density} & \text{Energy Flux } (x) & \text{Energy Flux } (y) & \text{Energy Flux } (z) \\ \text{Momentum Density } (x) & \text{Pressure } (x) & \text{Shear Stress } (xy) & \text{Shear Stress } (xz) \\ \text{Momentum Density } (y) & \text{Shear Stress } (yx) & \text{Pressure } (y) & \text{Shear Stress } (yz) \\ \text{Momentum Density } (z) & \text{Shear Stress } (zx) & \text{Shear Stress } (zy) & \text{Pressure } (z) \end{pmatrix}$$

Because those field equations are nonlinear partial differential equations that rarely admit closed-form analytical solutions, for most real-world scenarios, numerical solutions are needed. A survey of the known solutions of Einstein's field equations for vacuum, Einstein-Maxwell, pure radiation and perfect fluid sources can be found in [31]. The global properties of a number of exact solutions of Einstein's field equations are examined in [32]. The Schwarzschild metric is one well-known closed-form analytical solution [33]. It describes the geometry of spacetime surrounding a static (time-independent), spherically symmetric, uncharged mass in a vacuum where the energy-momentum tensor $T_{\mu\nu} = 0$. It solves the vacuum field equations $R_{\mu\nu} = 0$. In Schwarzschild coordi-

nates (t, r, θ, ϕ), the metric line element is $ds^2 = -\left(1 - \frac{2GM}{c^2 r}\right) c^2 dt^2 + \left(1 - \frac{2GM}{c^2 r}\right)^{-1} dr^2 + r^2(d\theta^2 + \sin^2\theta d\phi^2)$. The Schwarzschild radius $r_s = \frac{2GM}{c^2}$, a coordinate singularity, defines the event horizon of a non-rotating black hole, and a physical curvature singularity at $r = 0$ where the spacetime breaks down, that is, a true gravitational singularity. Numerical methods and large-scale simulations in relativistic systems where gravity plays a key role, such as black-hole formation, rotating stars, binary neutron-star evolution and even binary black-hole evolution, are described in [34]. The methods developed for numerical relativity, computational general relativity are central for the further study of the astrophysical universe, gravitational-wave astronomy and related fields of study.

Figure 6 summarizes the empirical validation of general relativity [35]. Due to a star's mass, in its vicinity there are extreme conditions in particular for the orbit of a planet around it. In the solar system that affects for example Mercury's orbit. Precession is the slow, continuous change in the orientation of a rotating body's axis of rotation and the path of its elliptical orbit. Figure 6(a) shows the conceptual difference in determining Mercury's orbital precession according to the Newtonian classical theory of gravity (top, closed loop) and general relativity (bottom, spiral). The former and latter theories calculated a precession of 531 and 574 arcseconds per century, respectively. Astronomers' observations confirmed only the one provided by general relativity. According to general relativity, massive celestial objects warp the fabric of spacetime around them. Gravitational lensing is an astrophysical phenomenon where those massive objects bend, magnify, and distort the path of light from a distant background source as it travels toward an observer. Figure 6(b) shows images provided with the Harvard-Smithsonian Center for Astrophysics (CfA)-Arizona Space Telescope Lens Survey (CASTLeS) [36]. They are false color images of the objects in question, based on radio observations, produced by a gravitational lens: (a) double quasar Q0957+561 (1979) (b) quasar QSO 2237+0305 (1985, Einstein cross) (c) type-2 quasar MG1131+0456 (1988, Einstein ring). Figure 6(c) shows black holes: in (i) warping the fabric of spacetime by the sun, by a white dwarf, by a neutron star, and by a black hole. In (ii) the black hole anatomy is displayed including the singularity, the event horizon, the photon sphere, the relativistic jets, the innermost stable orbit, and the accretion disc. In (iii) the first image of a black hole, the one at the center of the galaxy M87, is shown, taken using the Event Horizon Telescope, further details in [37]. Figure 6(d) shows the first detection of gravitational waves from the first observation of a binary black hole merger [38] accomplished using the twin observing stations located in Livingston (L1), Louisiana and Hanford (H1), Washington of the Laser Interferometer Gravitational-Wave Observatory (LIGO) [39] on September 14, 2015. The detected waves closely matched theoretical models of the black hole merger. The gravitational-wave event GW150914 observed involved black hole masses that merged some 1.3 billion years ago of initial $36^{+5}_{-4} M_\odot$ and $29^{+4}_{-4} M_\odot$, and the final was $62^{+4}_{-4} M_\odot$. The gravitational waves radiated $3.0^{+0.5}_{-0.5} M_\odot c^2$. Shown in (i) is the estimated gravitational-wave strain amplitude from GW150914 projected onto H1 (top) as well as the black hole separation in units of Schwarzschild radii and the effective black hole relative velocity (bottom). In (ii), the top and middle plots display the gravitational wave strain measured at the H1 detector (orange) and at the L1 detector (blue), respectively, alongside the theoretical predictions. The bottom plot displays the overlap of both detector signals after shifting the H1 data by a fraction of a millisecond to match the arrival time delay between the two sites, illustrating a close match. Finally, in (iii) screenshots of a computer visualization of the gravitational waves generated from the black hole merger are shown covering all phases, from inspiral to merger and ringdown.

Table 7: Classification of 1-manifolds

	without boundary: $\partial M = 0$	**with boundary:** $\partial M \neq 0$
Compact (finite)	circle: S^1	closed interval: $[0, 1]$
Non-compact (infinite)	real line: $\mathbb{R} = (-\infty, \infty)$ or $(0, 1)$	half-open interval: $[0, \infty)$ or $[0, 1)$

Next we discuss the Poincaré conjecture, originally stated in 1904 [40]. It is about the char-

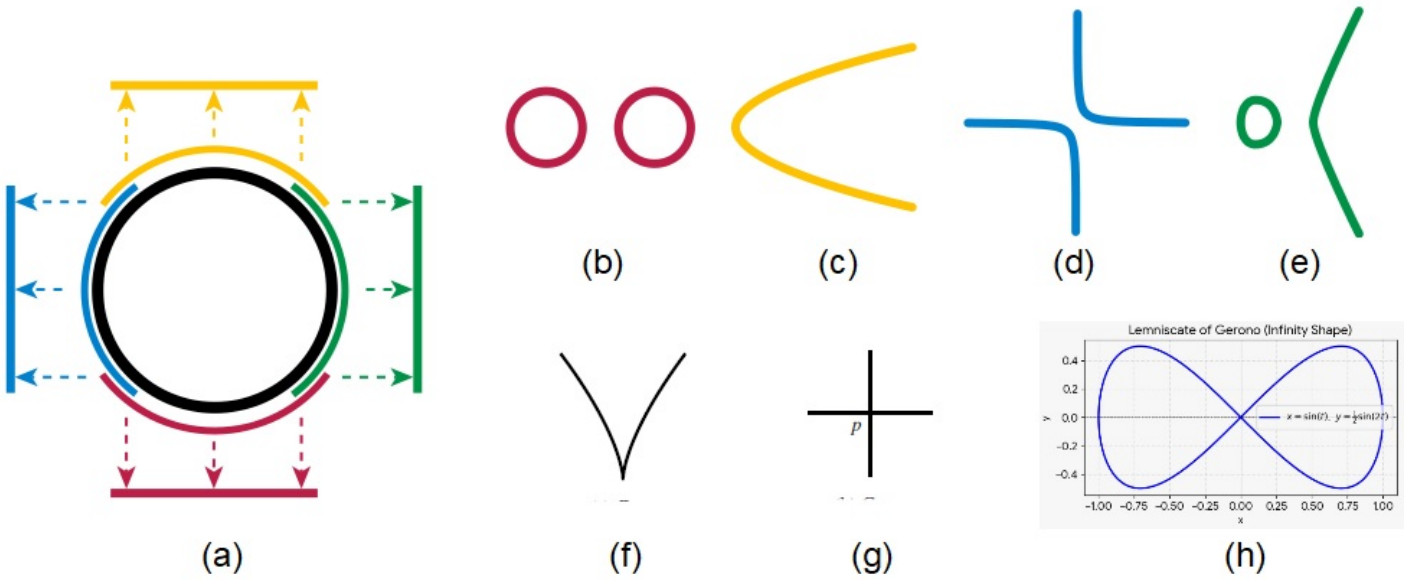

Figure 7: 1-manifolds (a) one circle (b) two circles (c) parabola (d) hyperbola (e) two-branch (one unbounded and one closed, oval) cubic curve (f) cusp (g) cross → is not (h) infinity → is not

acterization of the 3-sphere in the field of geometric topology. To gain understanding about issues involved, let us start with generalizations of the Poincaré conjecture, in 1- and 2- dimensions first. n-dimensional manifolds or n-manifolds, $n = 1, 2, 3, \cdots$, are topological spaces. Every point locally looks like: (1) for $n = 1$ (curve), like a line ($\mathbb{R}^1$), (2) for $n = 2$ (surface), like the 2-dimensional Euclidean space ($\mathbb{R}^2$), (3) for $n = 3$ (3-manifold), like the 3-dimensional Euclidean space ($\mathbb{R}^3$), etc. Depending on their dimension, manifolds possess extremely distinct structures, properties, and mathematical frameworks and tools to be handled with. 1-manifolds are relativiely straightforward to grasp. Figure 7 show example 1-manifolds (a–f) and figures that are not 1-manifolds (g–h). The circle in Figure 7(a), is a 1-manifold embedded in a two dimensional Euclidian space ($\mathbb{R}^2$). Infinitesimal circle arcs locally look like, resemble 1-dimensional line segments. Figure 7(b–d) show two circles, a parabola, and a hyperbola, respectively, all 1-manifolds. Figure 7(e) shows a two-branch cubic curve defined with $y^2 = x^3 - x$, which is also a 1-manifold, but neither the cusp defined with $y = x^{2/3}$, cf. Figure 7(f), nor the Lemniscate of Gerono (Figure-8 Curve) defined with: $x(t) = \sin(t), y(t) = \frac{1}{2}\sin(2t), t \in [0, 2\pi)$ or algebraically $x^4 - x^2 + y^2 = 0$, cf. Figure 7(h). Since a 1-manifold is a topological space that locally resembles the real line ($\mathbb{R}$) at every point, and that is not true for the cross and the Figure-8 curve due to their self-intersection points, they are not 1-manifolds. The 1-manifolds up to homeomorphism fall into four fundamental categories summarized in Table 7. Using point-set topology, it can be proved that up to homeomorphism, there are exactly four connected 1-manifolds [41]. An interval is a connected subset of $\mathbb{R}$ which is not a point. It may be finite or infinite; closed, open, or half-open. Another proof using the smooth category and the concept of parametrization by arc-length can be found in [42][Appendix], in its theorem about classifying 1-manifolds: Any smooth, connected 1-dimensional manifold is diffeomorphic either to the circle S^1 or to some interval of real numbers. Since any interval is diffeomorphic either to $[0, 1]$, $(0, 1]$, or $(0, 1)$, it follows that there are only four distinct connected 1-manifolds: the circle and these 3 intervals. Please note that the real line $\mathbb{R}$ is homeomorphic to the open interval $(0, 1)$ and the closed ray non-negative real numbers $[0, \infty)$ is homeomorphic to the half-open interval $[0, 1)$.

In two dimensions, there are orientable 2-manifolds and non-orientable 2-manifolds. In an orientable 2-manifold one can consistently define a global notion of clockwise when walking around a full loop, the same is true for being able to define a global notion of counterclockwise. In a non-orientable 2-manifold walking clockwise or counterclockwise around a full loop brings you back upside down. Figure 8 shows some examples of 2-manifolds including two orientable: the sphere

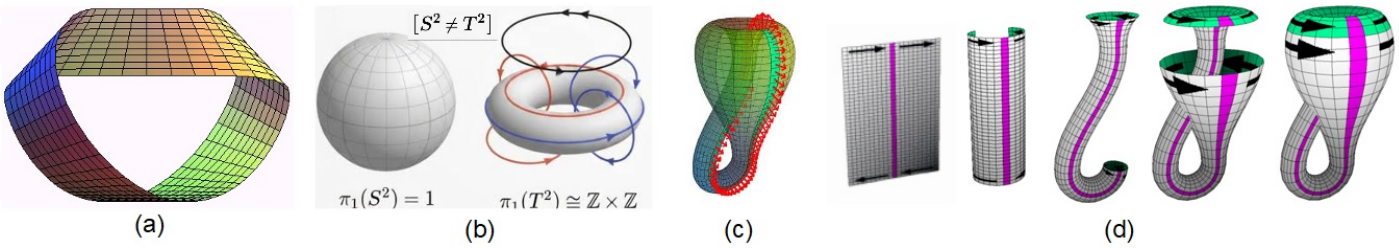

Figure 8: 2-manifolds (surfaces) (a) Möbius strip, non-orientable (b) sphere and torus are not homeomorphic, both orientable (c) Klein bottle, non-orientable (d) from a flat sheet to a Klein bottle

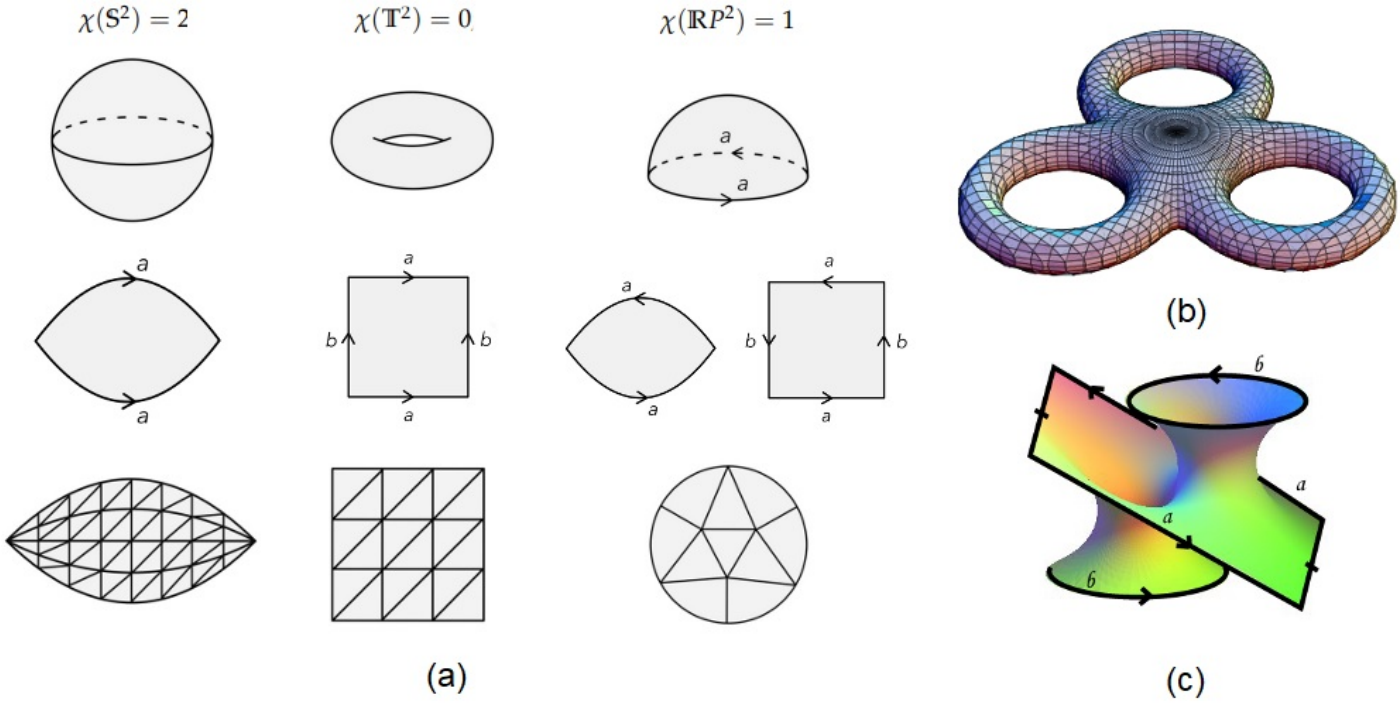

Figure 9: Standard surfaces and their connected sums (a) the 3 standard surfaces: sphere, torus, and real projective plane (b) triple torus as connected sum of 3 Tori (c) Dyck's surface as connected sum of 3 real projective planes

Table 8: Classification of 2-manifolds (surfaces)

surface type	**orientable**	**Euler characteristic** χ	**Standard Normal Form**
Sphere S^2	yes	2	aa^{-1}
$g-$fold Torus T_g	yes	$2-2g$	$a_1b_1a_1^{-1}b_1^{-1}\cdots a_gb_ga_g^{-1}b_g^{-1}$
$h-$fold real Projective Plane $\mathbb{R}P_h^2$	no	$2-h$	$a_1a_1a_2a_2\cdots a_ha_h$

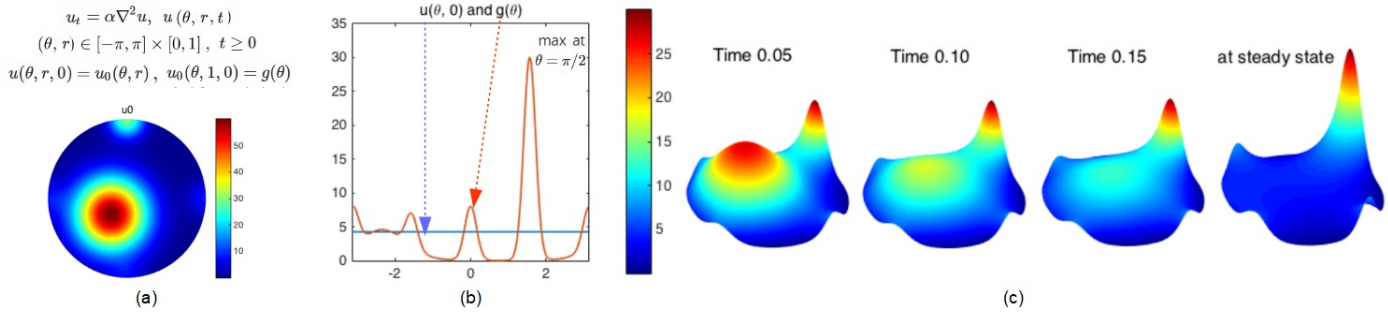

Figure 10: The heat equation and its solution example, underlying methods in [43] (a) top: equation, initial and boundary conditions, bottom: the initial heat profile u_0 consists of a sum of Gaussian bumps, the absolute maximum is in the interior of the disc (b) $g(\theta) = u_0(\theta, 1, t = 0)$, $\max(g)$ at $\theta = \pi/2$ (c) the solution function u is constructed numerically $\forall t \geq 0$, as the time t increases, the heat flows toward the hottest spot on the boundary of the disk

and the torus, and two non-orientable: the Möbius strip and the Klein bottle. For the last example it is also shown how starting from a flat sheet, a Klein bottle can be formed, by joining two sides of the sheet to form a cylinder first, then looping the ends of a cylinder back through itself in such a way that the inside (green) and outside (white) of the cylinder are joined. From the four examples, three: the sphere, the torus, and the Klein bottle are completely closed 2-manifolds and have no edges, boundary lines or endpoints. The Möbius strip has one continuous boundary edge. Figure 8(b) shows also why the sphere S^2 and the torus T^2 are not homeomorphic by showing that their fundamental groups used to measure the number of holes in a geometric shape are different: $\pi_1 = 0$ (simply connected, trivial group) and $\pi_1 = \mathbb{Z} \times \mathbb{Z}$ (ordered pairs of integers), respectively. In the case of the sphere, every loop can shrink to a point. In the case of the torus, loops can get stuck. The sphere, the torus, and the real projective plane are called standard surfaces.

In topology, spaces are homeomorphic if one can be continuously deformed into the other without tearing or gluing. If we define the 1-sphere (circle) as $S^1 = \{(x, y) \in \mathbb{R}^2 | x^2 + y^2 = 1\}$, the 2-torus as the Cartesian product of two circles $T^2 = S^1 \times S^1$, and $\mathbb{R}P^2$ is the real projective plane, then all orientable 2-manifolds are homeomorphic to the connected sum of g tori T^2 with $S_g = \sharp_g T^2 = T^2 \sharp \cdots \sharp T^2$, the $g-$fold connected sum of the 2-torus, $g \geq 0$ the genus of the 2-manifold and all non-orientable 2-manifolds are homeomorphic to the connected sum of h real projective planes $\mathbb{R}P^2$ with $R_h = \sharp_h \mathbb{R}P^2 = \mathbb{R}P^2 \sharp \cdots \sharp \mathbb{R}P^2$, the $h-$fold connected sum of $\mathbb{R}P^2$, $h \geq 1$ the genus or cross-cap number of the 2-manifold. We denote the connected sum of two surfaces, S_1 and S_2, as $S = S_1 \sharp S_2$, and the connected sum of two homeomorphic surfaces S_h as $S = 2S_h$. Compact, connected 2-manifolds (surfaces) are classified up to homeomorphism according to the classification theorem for surfaces: Every connected compact surface (2-manifold) without boundary is homeomorphic to either a sphere, or to a connected sum of tori, or to a connected sum of projective planes, see Table 8. The standard normal form column displays the corresponding canonical edge-labeling string of a polygon used to construct the topological surface via edge gluing. Figure 9 shows the standard surfaces (2-manifolds) and two examples of their connected sums. In Figure 9(a) we find three columns for each of the standard surfaces: sphere (left), torus (middle), and real projective plane (right). For each column, the following items are shown from top to bottom: its Euler characteristic χ, the surface itself, its polygonal representation, and its triangulation. Figure 9(a) and (b) show examples of the connected sum of standard surfaces, of three tori in (b) and of three real projective planes in (c). A rigorous proof of the surface classification theorem based on the polygon/word representation of triangulated surfaces was published in an article on analysis situs (topology) [44]. That every topological 2-manifold (surface) can be triangulated was then proven in [45]. A modern proof capturing Conway's Zero Irrelevancy Proof (ZIP) and bypassing polygon cutting-and-pasting entirely was presented in [46]. The subject has also been covered in textbooks including its treatment in [47] and more recently in [48].

Before we take the next partly AI-assisted – we could also state partly human-assisted – open

problem solution example, let us succinctly examine one entirely solved by human mathematicians. If we now take the Poincaré conjecture [40] and its resolution completed by G. Perelman [49, 50, 51], we can get a sense of the creativity of traditional, competent mathematicians' work, in particular how their theorem proof work looks like, with a high portion of creativity most would agree. The Poincaré conjecture states that every simply connected, closed 3-dimensional topological manifold is homeomorphic to the 3-dimensional sphere (S^3). The problem was solved using the Ricci flow with surgery, building upon a mathematical program originally developed by R. Hamilton in [52]. We now ourselves build upon what we know about the heat equation, that is, that the rate of change of the temperature at any given point is directly proportional to its spatial curvature and how we used Ricci's calculus to solve the Einstein's field equations of general relativity to now introduce and use the concept of Ricci flow. Heat naturally flows from regions of higher temperature to regions of lower temperature. Heat does not spread temperature through an object, what it does is deform and smooth out the curvature of the object's shape over time. Its core equation is $\frac{\partial u}{\partial t} = \alpha \nabla^2 u = \alpha \cdot \left(\frac{\partial^2 u}{\partial x^2} + \frac{\partial^2 u}{\partial y^2} + \frac{\partial^2 u}{\partial z^2} \right)$ with $u(x, y, z, t)$ the temperature at a given point (x, y, z) and time t, $\frac{\partial u}{\partial t}$ the rate of temperature change over time. ∇^2 the Laplacian, the sum of the second spatial derivatives, that measures the spatial curvature of the temperature distribution, $\alpha = \frac{k}{\rho c_p}$ the thermal diffusivity, k the thermal conductivity, ρ the density, and c_p the specific heat capacity. In order to solve that equation, we need initial and boundary conditions for the specific problem at hand. For example, Figure 10 shows the heat equation on a disk and its soluion. To solve this concrete example, the discretization in time (Δt) follows the second order accurate backward differentiation formula (BDF2), the underlying numerical methods to compute with functions in polar geometries for the disk can be found in [43] and the foundations for associated piecewise polynomial interpolation can be consulted in [53].

In a similar fashion, the Ricci flow deforms and smooths out geometric spaces, manifolds. The Ricci flow equation states: $\frac{\partial}{\partial t} g_{ij}(t) = -2R_{ij}$ with $g_{ij}(t)$ the components of the Riemannian metric tensor, which changes with time t, R_{ij} the components of the Ricci curvature tensor, which measures the degree to which the volume of geodesic balls in the curved space deviates from Euclidean space, the factor -2 is a convention to have the Ricci flow equation behave like a heat equation, smoothing out irregularities in the geometry. With that smoothing, and without singularities, complex three-dimensional objects could be broken down and straightened into standard shapes and that way, the Thurston geometrization conjecture could be proven. This much broader conjecture contains the Poincaré conjecture. Singularities are points where the space pinches off, tears or becomes infinitely curved stalling the equation. The Ricci flow is a natural evolution equation for Riemannian metrics on a given manifold. The classification of models of singularity formation in dimension 3 is discussed in [54]. In particular, every finite-time singularity to the Ricci flow in dimension 3 is modeled on an ancient $\kappa-$solution as shown in [49]. This ancient solution is a smooth, nonflat, maximal solution to the Ricci flow equation that satisfies four criteria: to be ancient, complete and bounded, to have nonnegative curvature, and to be $\kappa-$noncollapsed. For r (scale), points given by (x, t), P a parabolic ball, V volume of a geodesic ball, the last condition listed states in formal terms: $\forall r > 0, (x, t) \in P(x, t, , r, -r^2), \exists \kappa : (R \leq r^{-2} \Rightarrow V_{g(t)}(B_{g(t)}(x, r)) \geq \kappa r^n)$. In dimension $n = 3$, these solutions are the universal models for finite-time singularities and are completely classified as either the shrinking round sphere S^3, the shrinking cylinder $S^2 \times \mathbb{R}$, or their quotients and unique asymmetric variations like the Bryant soliton. The $\kappa-$noncollapsing condition prevents the Ricci flow from developing infinite, thin tubes or sharp cusps where the curvature explodes while the local volume drops to zero. Without this condition, a singularity could pinch down so tightly that the manifold collapses into a lower-dimensional state locally, making it mathematically impossible to analyze or restart the flow. The prevention strategy controls local volume that guarantees that if the curvature is controlled within a certain radius $R \leq r^{-2}$, the volume of that region cannot be arbitrarily small. It must scale proportionally to a baseline fraction κ of standard Euclidean space. The strategy forces geometric rigidity. Because the volume is bounded away from zero, blowing up, zooming in on the singularity forces the geometry to look like a smooth, well-behaved limit rather

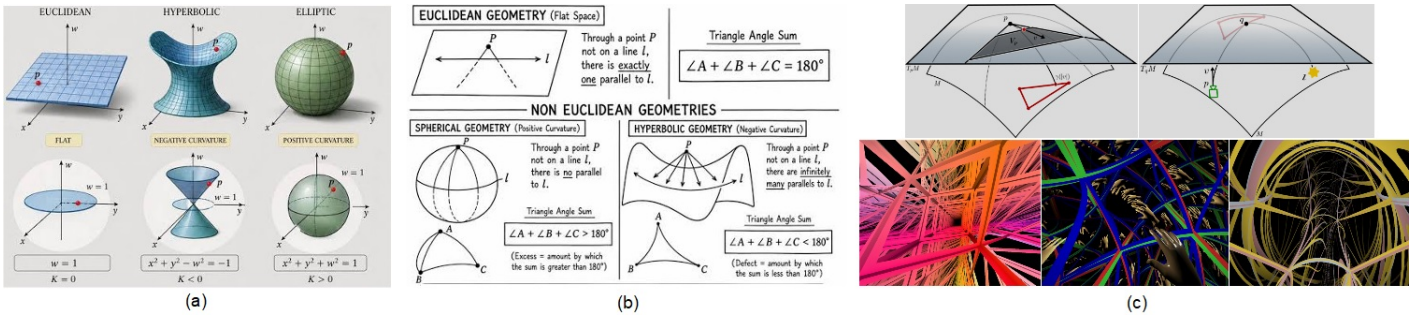

Figure 11: Three geometries (one Euclidian, two non-Euclidian), three curvatures (a) $\kappa = 0$ (flat), $\kappa < 0$ (negative curvature), $\kappa > 0$ (positive curvature) (b) for Euclidian, spherical, hyperbolic geometry, respectively: given point P and line l, number of parallel lines to l through $P : 1, 0, \infty$, triangle angle sum: $=, >, < 180°$ (c) visualization of Thurston geometries, top: tracing rays in a Riemannian manifold M (left), the hit point q is connected with the light source l through a geodesic (right), bottom: inside view of a manifold: $\widetilde{\mathrm{PSL}(2, \mathbb{R})}$ (left), Nil (middle), Sol (right) [60]

than a chaotic, infinitesimal needle. The strategy also enables geometric surgery. By ensuring that every singularity looks like a thick, predictable geometric shape, i.e., like a sphere or a solid cylinder, Perelman proved that one can perform surgery, i.e., can safely cut out the singularity and glue in a smooth cap to continue the flow.

The Thurston geometrization conjecture states that every closed, orientable 3-manifold can be decomposed in a canonical way, via topological decompositions of 3-manifolds: prime Kneser-Milnor [55, 56] and Jaco–Shalen–Johannson (JSJ) [57, 58] into pieces, each of which admits a geometric structure modeled on one of eight Thurston geometries [59]: two of the three constant curvature ones $\mathbb{S}^3$ (Spherical), $\mathbb{R}^3$ (Euclidian), the other four Seifert-fibered ones $\widetilde{\mathrm{PSL}(2, \mathbb{R})}, \mathbb{H}^2 \times \mathbb{R}, \mathbb{S}^2 \times \mathbb{R}$, Nil, as well as $\mathbb{H}^3$ (Hyperbolic, constant curvature), and Sol. $\mathrm{PSL}(2, \mathbb{R})$ is the Projective Special Linear group of 2×2 matrices over the real numbers, after $\sim$-twisting: $ds^2 = \frac{dx^2+dy^2}{y^2} + (dz + \frac{dx}{y})^2$ topologically homeomorphic to an open solid cylinder ($\mathbb{D}^2 \times \mathbb{R}$). The Nil and Sol geometries have as underlying space $\mathbb{R}^3$ and are modeled on the 3-dimensional Heisenberg group ($ds^2 = dx^2 + dy^2 + (dz - xdy)^2$) and on a solvable 3-dimensional Lie group ($ds^2 = e^{-2z}dx^2 + e^{2z}dy^2 + dz^2$), respectively. Figure 11 shows the three constant curvature Thurston geometries and the visualization of two Seifert-fibered Thurston geometries and Sol.

The shrinking round sphere S^3 is a hypersphere in three dimensions that you can picture as a family of concentric 2-spheres that swell from a single point, reach a maximum equator size, and taper back down to a point. Under Ricci flow, every single point curves inward identically, forcing the volume to instantly collapse into a singularity. The shrinking cylinder $S^2 \times \mathbb{R}$ that represents a standard three dimensional neck pinch and you can visualize as a long, infinite straight pipe. The circular cross-section is a 2-sphere S^2 and the infinite pipe length is the real line $\mathbb{R}$. Under Ricci flow, curvature only exists along the round walls, causing the pipe's radius to pinch downward rapidly over time. The straight line direction $\mathbb{R}$ experiences no Ricci curvature, so it does not contract lengthwise. It models the throat of a barbell shape during a neck pinch. According to the geometrization theorem, every closed 3-manifold can be canonically decomposed into pieces, each of which possesses one of eight distinct Thurston geometric structures. Figure 12(a) shows conceptually Ricci flow on a two dimensional manifold. Then in (b), a shrinking round sphere S^3 (top) and a shrinking cylinder $S^2 \times \mathbb{R}$ (bottom) are displayed outlining its main components, the way we can imagine they are structured since they cannot be directly displayed in Euclidian space. Finally, in (c) 3-manifolds are gathered in a table in relation to the solution of the Thurston geometrization conjecture. In the case of the proof of the Thurston geometrization conjecture and with it of the Poincaré conjecture (a smaller, specific case), the larger theorem provides a complete classification system for all three dimensional shapes, i.e. 3-manifolds, a table including all possible three dimensional geometries. This definitely changes our view of the geometry of 3D space and how we approach the study of shape, not only confirming the

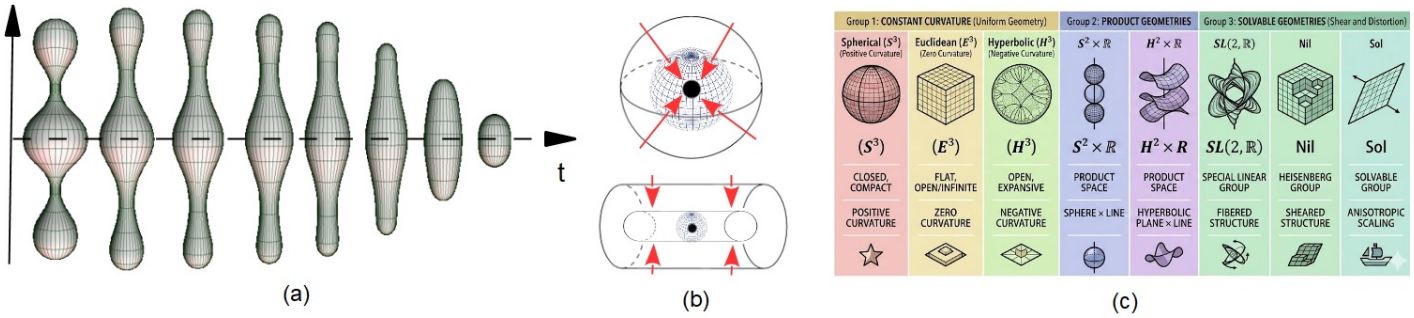

Figure 12: Thurston geometrization conjecture (a) stages of the Ricci flow on a two dimensional manifold (b) shrinking round sphere S^3 (top) and shrinking cylinder $S^2 \times \mathbb{R}$ (bottom) (c) 3-manifolds: the 8 Thurston geometric structures

uniqueness of the 3-sphere. The human mathematician, in this case Perelman, expanded Hamilton's work using Ricci flow creating, constructing novel analytical tools to smooth out irregularities and expose, reveal the true underlying geometric structures of rough spaces. Therefore, his work can be considered without a doubt a geometrization breakthrough.

In recent years, AI has become increasingly capable in mathematics, for some observations about how AI is changing math and science forever, see e.g. [61][Chapter 3]. In particular, AI has become genuinely useful in assisting tasks like literature searches, proofreading, writing some code, and verifying a proof. Currently, its advanced mathematics capabilities are being further improved to tackle and solve more complex problems like the above-mentioned unit distance conjecture. Automated proof indigestion refers to the fact that the human verification of fast-paced AI-generated mathematics results, is at least currently not straightforward, demands substantial effort and time. While human mathematicians continue learning how to use AI as assistant, there has been some negative effect for the mathematics community through a controversy recently reported among others in [62]. OpenAI claims to have solved under the guidance of a team of mathematicians and using an unreleased internal model, a massive multi-agent AI system, one of the 7 CMI millenium prize problems: the Navier-Stoke existence and smoothness problem. There is no certainty whether they had unallowed access to results or data used for training from the work jointly produced by T. Buckmaster, NYU Courant Institute and L. Alpöge, Anthropic. From [63]: "Once we saw the Euler solution, we thought that Navier–Stokes was the most promising problem to work on. Thus, we decided to devote our resources to Navier–Stokes. To do so, we shifted agents away from the other Millennium Problems and prompted these agents with the Euler resolution". Due to this uncleared incident after direct interaction between both parties, the latter group had to publish a preliminary version of their work including about the forced three-dimensional incompressible Euler equations in [64] and its Lean formal verification in [65]. The OpenAI proof uses a counterexample showing finite-time singularity breakdown (velocity blowup) with an external force, and provides a writeup of the proof [66] as well as its formalization in Lean [67]. Figure 13 shows the description of fluid motion according to the three-dimensional incompressible Navier–Stokes equations and the OpenAI's answer to the fundamental question whether a solution starting from smooth data can develop unbounded velocity in finite time while its kinetic energy remains bounded. The construction of the solution flow is done with zero initial velocity and a smooth force compactly supported in space and time resulting in a vortex, a spinning swirl of fluid, that spirals inward and gets increasingly elongated. This vortex resolves the formulation of the Navier–Stokes millennium prize problem as posed in [68] proving statements (C) and (D) therein, for the award only one of four option proofs is needed. The velocity field is shown in (a), the factors influencing the parcel's motion in (b). the gradual singularity formation in (c), and a corresponding three-dimensional rendering in (d), where orange denotes faster angular rotation. Autoformalization has become a popular method used to verify mathematical texts, including those generated by AI. For that purpose, another AI system translates the text from a natural language (NL) into a formal language such as Lean to obtain a formal proof. The argument expressed in the formal

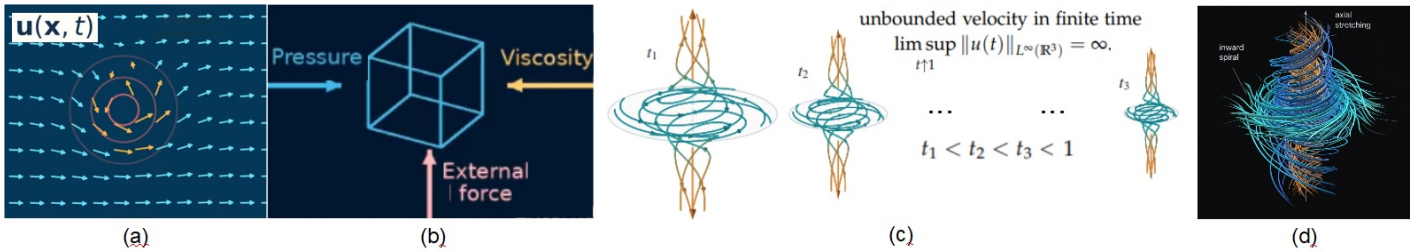

Figure 13: Three-dimensional incompressible Navier Stokes equations (a) velocity field $\mathbf{u}(\mathbf{x}, t)$ (b) factors influencing parcel's motion (c) unbounded velocity in finite time (d) 3D conceptual rendering [OpenAI]

language is then mechanically verified, but this process may not offer confidence in the original NL argument, due to complexities performing the translation semantically faithfully. Examples of AI mistranslations of NL statements and proofs into Lean in practice, resulting in mismatches between NL proofs and their Lean verifications are discussed in [69]. These include OpenAI's recently released Navier-Stokes proof, specifically showing that the formalized Lean proof does not correspond to the NL proof of blowup of solutions to the Navier-Stokes equations. The underlying approach to solve the here discussed Navier-Stokes problem has been the construction of forced blowups, introduced by D. Córdoba and L. Martínez-Zoroa, for example for the forced 3D incompressible Euler equations [70]: $\partial_t u + (u \cdot \nabla)u + \nabla p = f, \nabla \cdot u = 0, u_0(x) = u(x, 0)$ with $u(x, t)$ the velocity field, $p(x, t)$ the pressure function of an ideal fluid, and f an external force; and for the hypodissipative ($0 < \alpha < 2$) forced fractional Navier Stokes equations [71]: $u_t + u \cdot \nabla u + \nabla p + \nu|\nabla|^\alpha u = f, (x, t) \in \mathbb{R}^3 \times \mathbb{R}_t, \nabla \cdot u = 0, u_0 = u(x, 0)$ with $u(x, t)$ the velocity field, $p(x, t)$ the pressure function, $\nu > 0$ the viscosity coefficient, and f an external force.

There is no consensus on how AI is currently viewed in the mathematics community. For example, it is partly viewed by some applied mathematicians as an empowering instrument, maybe compared to a telescope or microscope, and by some pure mathematicians with substantial practical concern that machine-generated proofs are for the most shallow, unreadable, or mass-produced formalisms and does not foster human intellectual skills, especially for students at any level in the meantime. Transferring somehow from a state of proof scarcity to proof abundance and proof digestion has not been received by all with great enthusiasm. Proofs need to be reviewed by humans and need to be well understood, and that takes substantial time and change of habits. On the other hand, there is growing recognition that it could assist us, currently still under human guidance and supervision, tackle challenging open problems. That is why some see themselves forced to a fundamental cultural and practical shift across the discipline. Because some of the most notable accomplishments were reported to have been done using internal proprietary frontier AI models, unreleased to the general public, mathematicians have not been easily convinced since they cannot reproduce the results, it is not only about verifying them. There is no doubt that the potential is huge, only how far the AI competence and assistance can reach is to this date not quite clear yet. And there is also a major issue about the intellectual property (IP) of human generated results or even AI intrusion into human's work without proper authorization, mainly because of partly irresponsible operations and insufficient safety and security mechanisms of AI system hardware and software. Due to the fast progress in the research and technology development of Artificial Intelligence (AI) and Machine Learning (ML), new names have emerged including Artificial General Intelligence (AGI) and Artificial Super Intelligence (ASI) [72], more recently Super Intelligence (SI) [73], and intermediate steps, now fully operational, towards those associated goals are Generative AI (GenAI) and Agentic AI [74]. Unauthorized incursions of AI agentic systems into competitor or even customer enterprise IT has been reported, see e.g. [75]. Thus, the demand for regulatory governance and technical improvements in the security and safety of advanced AI systems, in hardware and software, has grown and been recently addressed in [76]. Debates concerning the cost-benefit trade-offs of deploying autonomous AI systems extend well beyond mathematics circles. Organizations are currently deploying agentic coding tools and coming to terms with the costs of AI while still seeking to

capture more of the benefits that their employees are deriving from their individual use of AI [77]. The abstraction power of mathematics enables the definition of core functionalities for advanced autonomous AI systems with high degree of versatility in their application. That leads to diverse requirements for proper advanced AIOps [78]. In this report most if not all aspects of the impact of AI advancements in mathematics and beyond are explored in technical depth. In particular, the crucial shift of human involvement, current and future, by no means necessarily sidelining. Multiple avenues of accelerated AI progress, currently not broadly available in AI systems, are described, presenting fully autonomous AI system implementations that operate at the push of a button. These systems tackle complex tasks in mathematics and beyond, which require a high degree of creativity, ultimately serving the invention of the next generation technologies and systems in all areas of human endeavor. The work in this report is an integral part of the preparation phase to launch a new Institute of Advanced Artificial Super Intelligence (AASI).

References

[1] V.D. Sánchez. *Neurocomputing 50th volume anniversary*. Neurocomputing, 50, ix, 2003. https://profdrvdsaphd.lima-city.de/documents/Neurocomputing50thAnniversary.pdf

[2] V.D. Sánchez. *IEEE Fellow Award – "for leadership in neural and parallel computation, and pioneering contributions to autonomous space robots"*. 1995. https://profdrvdsaphd.lima-city.de/documents/IEEEFellow.pdf

[3] V.D. Sánchez. *Personal written communication with the Office of the German Federal Minister of Research and Technology BMFT – Start of the First German National AI/ML Research and Technology Development Program*. 1988.

[4] D. Hilbert. *Mathematische Probleme*. Nachrichten von der Königl. Gesellschaft der Wissenschaften zu Göttingen, Mathematisch-physikalische Klasse, Heft 3, S. 253–297, 1900

[5] Associate Editors of Mathematical Reviews (MR) and Zentralblatt für Mathematik (zbMATH). *Mathematics Subject Classification (MSC) System*. 2020. https://msc2020.org/MSC_2020.pdf

[6] The Norwegian Academy of Science and Letters. *The Abel Prize*. https://abelprize.no/

[7] International Mathematical Union. *Fields Medal*. https://www.mathunion.org/imu-awards/fields-medal

[8] The Breakthrough Prize Foundation. *The Breakthrough Prize*. https://breakthroughprize.org/

[9] V.D. Sánchez. *Künstliche Intelligenz und Maschinelles Lernen zur Lösung ungelöster Probleme in der Mathematik*. März 2025. https://profdrvdsaphd.lima-city.de/documents/ArtificialGeneralIntelligenceMachineLearningOnMathematics.pdf

[10] M. Gerwig. *Der Satz des Pythagoras in 365 Beweisen*. Springer Verlag, 2021.

[11] Lean. *Open-source progamming language and proof assistant*. October 2026. https://lean-lang.org/

[12] P. Erdős. *On sets of distances of n points*. American Mathematical Monthly, 53 (1946) 5, 248–250.

[13] OpenAI. *An OpenAI model has disproved a central conjecture in discrete geometry*, May 20, 2026. https://openai.com/index/model-disproves-discrete-geometry-conjecture/

[14] OpenAI. *Planar Point Sets with Many Unit Distances*, May 20, 2026. https://cdn.openai.com/pdf/74c24085-19b0-4534-9c90-465b8e29ad73/unit-distance-proof.pdf

[15] F. Hajir and C. Maire. *Asymptotically good towers of global fields*. In C. Casacuberta et al. (Eds), European Congress of Mathematics, Vol. II (Barcelona, 2000), vol. 202 of Progress in Mathematics, 207–218. Birkhäuser, 2001.

[16] F. Hajir et al. *Cutting towers of number fields*. Annales Mathématiques du Québec, 45 (2021) 2, 321–345.

[17] J. Neukirch. *Algebraische Zahlentheorie*. Springer, 1992.

[18] B. Alexeev et al. *The Erdös unit distance problem for small point sets*. February 12, 2025. https://arxiv.org/pdf/2412.11914

[19] ChatGPT. *Simplified Unit Distance Visualizer*. October 2026. https://chatgpt.com/canvas/shared/6a15da73c5b08191a2dc34c3ac6ceca6

[20] V.D. Sánchez. *Searching for a solution to the automatic RBF network design problem*. Neurocomputing, 42 (1-4), 147–170, 2002.

[21] V.D. Sánchez. *Beiträge zum überwachten Lernen reellwertiger Funktionen mithilfe neuronaler Netze*. Deutsches Zentrum für Luft- und Raumfahrt (DLR) Bericht, unveröffentlicht, 1993.

[22] V.D. Sánchez. *AI/ML Methods to Develop Superior Next Gen Autonomous Learning Robot Systems for Industrial Terrestrial and Space Applications*. December 2024. https://profdrvdsaphd.limacity.de/documents/AIMLNextGenAutonLearnRobots.pdf

[23] V.D. Sánchez. *Analysis and Implementation of Heuristical Algorithms for Two-Level Logic Minimization of Digital Circuits, 3 volumes (in German)*. Final Report, Karlsruhe Institute of Technology (KIT), February 1986.

[24] A.L. Blum and R.L. Rivest. *Training a 3-Node Neural Network is NP-Complete*. in S.J. Hanson et al (Eds): Machine Learning: From Theory to Applications: Cooperative Research at Siemens and MIT. Springer 1993, 9–28.

[25] M. Minsky and S. Papert. *Perceptrons – An Introduction to Computational Geometry*. Expanded Edition. The MIT Press 1988.

[26] W.v.O. Quine. *The Problem of Simplifying Truth Functions*. The American Mathematical Monthly, 59 (1952) 8, 521–531.

[27] E.J. McCluskey Jr. *Minimization of Boolean functions*. Bell System Technical Journal 35 (1956) 6, 1417–1444.

[28] B. Dunham and R. Fridshal. *The Growth of Complexity of Prime Implicants*. Journal of the ACM (JACM), 6 (1959) 4, 559–560.

[29] M.R. Garey and D.S. Johnson. *Computers and Intractability: A Guide to the Theory of NP-Completeness*. W. H. Freeman, 1979.

[30] G. Ricci and T. Levi-Civita. *Méthodes de calcul différentiel absolu et leurs applications*. Mathematische Annalen 54 (1900) 1–2, 125–201.

[31] S.H. Kramer et al. *Exact Solutions of Einstein's Field Equations*. 2nd Edition. Cambridge University Press, 2003.

[32] S.W. Hawking et al. *The Large Scale Structure of Space-Time*. Cambridge University Press, 1975.

[33] K. Schwarzschild. *Über das Gravitationsfeld eines Massenpunktes nach der Einsteinschen Theorie*. Sitzungsberichte der Königlich Preussischen Akademie der Wissenschaften, 1916, 189–196.

[34] T.W. Baumgarte and S.L. Shapiro. *Numerical Relativity. Solving Einstein's Equations on the Computer*. Cambridge University Press, 2011.

[35] V. Ferrari et al. *General Relativity and its Applications – Black Holes, Compact Stars and Gravitational Waves*. CRC Press 2026.

[36] Harvard-Smithsonian Center for Astrophysics (CfA). *CASTLES Survey*. 2026. https://lweb.cfa.harvard.edu/castles/

[37] NASA. *First Image of a Black Hole*. 2026. https://science.nasa.gov/resource/first-image-of-a-black-hole/

[38] B.P. Abbott et al. *Observation of Gravitational Waves from a Binary Black Hole Merger*. Phys. Rev. Lett. 116, 061102, 11 February, 2016.

[39] LIGO. *Laser Interferometer Gravitational-Wave Observatory – Timeline*. 2026. https://www.ligo.caltech.edu/page/timeline

[40] H. Poincaré. *Cinquième complément à l'analyse situs*. Rendiconti del Circolo Matematico di Palermo 18 (1904): 45–110.

[41] D. Gale. *The Classification of 1-Manifolds: A Take-Home Exam*. Journal of The American Mathematical Monthly, 94 (1987) 2, 170–175.

[42] J. Milnor. *Topology from the Differentiable Viewpoint*. 1965.

[43] H. Wilber. *Computing with functions in spherical and polar geometries II. The disk*. SIAM Journal on Scientific Computing 39 (2017) 3, C238–C262.

[44] M. Dehn and P. Heegaard. *Analysis Situs*. Encyklopädie der Mathematischen Wissenschaften mit Einschluss ihrer Anwendungen, IIIAB1(3), 153–220, 1907.

[45] T. Radó. *Über den Begriff der Riemannschen Fläche*. Acta Litterarum ac Scientiarum Regiae Universitatis Hungaricae Francisco-Josephinae. Sectio Scientiarum Mathematicarum (Acta Szeged), 2 (1925) 2, 101–121.

[46] G.K. Francis and J.K. Weeks. *Conway's ZIP Proof*. The American Mathematical Monthly, 106 (1999) 5, 393–405.

[47] H. Seifert and W. Threlfall. *Lehrbuch der Topologie*. B.G. Teubner 1934.

[48] J. Gallier and D. Xu. *A Guide to the Classification Theorem for Compact Surfaces*. Springer 2013.

[49] G. Perelman. *The entropy formula for the Ricci flow and its geometric applications*. 2002. https://arxiv.org/pdf/math/0211159

[50] G. Perelman. *Ricci flow with surgery on three-manifolds*. 2003. https://arxiv.org/pdf/math/0303109

[51] G. Perelman. *Finite extinction time for the solutions to the Ricci flow on certain three-manifolds*. 2003. https://arxiv.org/pdf/math/0307245

[52] R.S. Hamilton. *Three-manifolds with positive Ricci curvature*. Journal of Differential Geometry 17 (1982) 3, 255–306.

[53] L.N. Trefethen. *Approximation Theory and Approximation Practice*. Extended Edition. Society for Industrial and Applied Mathematics (SIAM) 2019.

[54] S. Brendle. *Singularity models in the three-dimensional Ricci flow*. 2022. https://arxiv.org/pdf/2201.02522

[55] H. Kneser. *Geschlossene Flächen in dreidimensionalen Mannigfaltigkeiten*. Jahresbericht der Deutschen Mathematiker-Vereinigung 38 (1929), 248–260.

[56] J. Milnor. *A Unique Decomposition Theorem for 3-Manifolds*. American Journal of Mathematics 84 (1962) 1, 1–7.

[57] W. Jaco and P. Shalen. *Seifert Fibered Spaces in 3-Manifolds*. Memoirs of the American Mathematical Society Volume: 21, Number 220, September 1979.

[58] K. Johannson. *Homotopy Equivalences of 3-Manifolds with Boundaries*. Lecture Notes in Mathematics, Vol. 761, 1979.

[59] W.P. Thurston. *Three dimensional manifolds, Kleinian groups and hyperbolic geometry*. Bulletin of the American Mathematical Society 6 (1982) 3, 357–381.

[60] T. Novelloa et al. *How to see the eight Thurston geometries*. 14 September 2021. https://arxiv.org/pdf/2005.12772

[61] T. Tao. *Six Math Essentials*. Quanta Books, 2026.

[62] Scientific American. *OpenAI claims blockbuster math breakthrough amid swirl of controversy*. September 8, 2026. https://www.scientificamerican.com/article/openai-claims-blockbuster-math-breakthrough-amid-swirl-of-controversy/

[63] OpenAI. *On the Navier–Stokes Millennium Prize Problem*, September 8, 2026. https://openai.com/index/navier-stokes-solution/

[64] L. Alpöge and T. Buckmaster. *Blowup for the Euler equations with smooth forcing*. 2026. https://cims.nyu.edu/ tristanb/euler.pdf

[65] T. Buckmaster and L. Alpöge. *Finite-time blow-up for the three-dimensional incompressible Euler equations with smooth force — Lean 4 formalisation*. September 8, 2026. https://github.com/tristanbuckmaster/fluid_lean/tree/main/euler-blowup

[66] OpenAI. *Finite time blowup for Navier–Stokes*, September 8, 2026. https://cdn.openai.com/pdf/32d9f210-8b73-45e0-91bc-82a30aef8a9a/navier-stokes.pdf

[67] OpenAI. *Lean certificates accompanying Navier-Stokes and Euler results*, September 8, 2026. https://github.com/openai/NavierStokesAndEuler

[68] C.L. Fefferman. *Existence and smoothness of the Navier–Stokes equation*. Clay Mathematics Institute, Millennium Prize Problem statement. https://www.claymath.org/wp-content/uploads/2022/06/navierstokes.pdf

[69] A. Bastounis et al. *Navier–Stokes lost in translation – Why Lean verification of AI autoformalisation does not guarantee correct natural language proofs*. 6 October 2026. https://arxiv.org/html/2610.08144v1

[70] D. Córdoba and L. Martínez-Zoroa. *Blow-up for the incompressible 3D-Euler equations with uniform $C^{1,\frac{1}{2}-\varepsilon} \cap L^2$ force*. 15 September 2023. https://arxiv.org/pdf/2309.08495

[71] D. Córdoba et al. *Finite time blow-up for the hypodissipative Navier Stokes equations with a force in $L^1_t C^{1,\epsilon}_x \cap L^\infty_t L^2_x$*. 5 August 2024. https://arxiv.org/pdf/2407.06776

[72] V.D. Sánchez. *On Artificial General Intelligence (AGI) and Artificial Super Intelligence (ASI)*. January 2025. https://profdrvdsaphd.lima-city.de/documents/OnArtificialGeneralIntelligenceAndArtificialSuperIntelligence.pdf

[73] The White House, Presidential Actions, Executive Order. *Inaugurating The Era Of Super Intelligence*, September 29, 2026 . https://www.whitehouse.gov/presidential-actions/2026/09/inaugurating-the-era-of-super-intelligence/

[74] V.D. Sánchez. *Architecting Next-Generation Generative AI/ML Models and Agentic AI Solutions*. August 2025. https://profdrvdsaphd.lima-city.de/documents/ArchitectingNextGenAIMLAgenticAISolutions.pdf

[75] Hugging Face. *Anatomy of a frontier-lab agent intrusion*, July 27, 2026. https://huggingface.co/blog/agent-intrusion-technical-timeline

[76] V.D. Sánchez. *The Necessity of Artificial Intelligence (AI) Regulatory Governance, Shielding National Security Assets, and the Birth of the Brand Super Intelligence (SI)*. September 2026. https://profdrvdsaphd.lima-city.de/documents/AIRegGovShieldNatSecAssetsSI.pdf

[77] McKinsey & Company. *The State of AI in 2026 – On the Road to ROI*. August 2026.

[78] V.D. Sánchez. *Advanced Automation for mission-critical Information Technology past AIOps*. November 2024. https://profdrvdsaphd.lima-city.de/documents/AdvancedAutomationMisCriITPastAIOps.pdf